

3D periodic dielectric composite homogenization based on the Generalized Source Method

Alexey A. Shcherbakov,^{1,*} and Alexandre V. Tishchenko²

¹Laboratory of Nanooptics and Plasmonics, Moscow Institute of Physics and Technology, 9 Institutsky, Dolgoprudny, 141707, Russia

²Laboratory Hubert Curien, University of Lyon, Bâtiment F, 18 Rue Professeur Benoît Lauras, Saint-Etienne, 42000, France

*alex.shcherbakov@phystech.edu

Abstract: The article encloses a new Fourier space method for rigorous optical simulation of 3D periodic dielectric structures. The method relies upon rigorous solution of Maxwell's equations in complex composite structures by the Generalized Source Method. Extremely fast GPU enabled calculations provide a possibility for an efficient search of eigenmodes in 3D periodic complex structures on the basis of rigorously obtained resonant electromagnetic response. The method is applied to the homogenization problem demonstrating a complete anisotropic dielectric tensor retrieval.

OCIS codes: (050.1755) Computational electromagnetic methods; (050.2065) Effective medium theory; (050.5298) Photonic crystals; (050.6624) Subwavelength structures.

References and links

1. M. D. Turner, et. al., "Miniature chiral beamsplitter based on gyroid photonic crystals," *Nature Photon.* **7**, 801-805 (2013).
2. M. Faryad, A. Lakhtakia, and D. P. Pulsifer, "Dyakonov–Tamm waves guided by the planar surface of a chiral sculptured thin film," *J. Opt. Soc. Am. B* **30**, 3035-3040 (2013).
3. V. Yu. Timoshenko, L. A. Osminkina, A. I. Efimova, L. A. Golovan, and P. K. Kashkarov, "Anisotropy of optical absorption in birefringent porous silicon," *Phys. Rev. B* **67**, 113405 (2003).
4. M. Thiel, M. S. Rill, G. von Freymann, and M. Wegener, "Three-dimensional bi-chiral photonic crystals," *Adv. Mater.* **21**, 4680-4682 (2009).
5. M. Deubel, et. al., "Direct laser writing of three-dimensional photonic-crystal templates for telecommunications," *Nature Mater.* **3**, 444-447 (2004).
6. R. Tao, Z. Chen, and P. Sheng, "First-principles Fourier approach for the calculation of the effective dielectric constant of periodic composites," *Phys. Rev. B* **41**, 2417-2420 (1990).
7. S. Datta, C. T. Chan, K. M. Ho, and C. M. Soukoulis, "Effective dielectric constant of periodic composite structures," *Phys. Rev. B* **48**, 14936-14943 (1993).
8. V. A. Markel, and J. C. Schotland, "Homogenization of Maxwell's equations in periodic composites: boundary effects and dispersion relations," *Phys. Rev. E* **85**, 066603 (2012).
9. P. Lalanne, "Effective medium theory applied to photonic crystals composed of cubic or square cylinders," *Appl. Opt.* **35**, 5369-5380 (1996).
10. R. D. Meade, A. M. Rappe, K. D. Brommer, J. D. Joannopoulos, and O. L. Alerhand, "Accurate theoretical analysis of photonic band-gap materials," *Phys. Rev. B* **48**, 8434-8437 (1993).
11. S. G. Johnson, and J. D. Joannopoulos, "Block-iterative frequency-domain methods for Maxwell's equations in a planewave basis," *Opt. Expr.* **8**, 173-190 (2001).
12. S. Guo, and S. Albin, "Simple plane wave implementation for photonic crystal calculations," *Opt. Expr.* **11**, 167-175 (2003).
13. A. A. Shcherbakov, A. V. Tishchenko, "New fast and memory-sparing method for rigorous electromagnetic analysis of 2D periodic dielectric structures," *J. Quant. Spectrosc. Radiat. Transfer* **113**, 158-171 (2012).
14. A. A. Shcherbakov, A. V. Tishchenko, "Efficient curvilinear coordinate method for grating diffraction simulation," *Opt. Express* **21**, 25236-25247 (2013).
15. A. V. Tishchenko, "A generalized source method for wave propagation," *Pure Appl. Opt.* **7**, 1425-1449 (1998).
16. L. B. Felsen, and N. Marcuvitz, *Radiation and Scattering of Waves* (Wiley-IEEE Press, 2001).
17. J. A. Schmalz, G. Schmalz, T. E. Gureyev, and K. M. Pavlov, "On the derivation of the Green's function for the Helmholtz equation using generalized functions," *Am. J. Phys.* **78**, 181-186 (2010).

18. E. Popov, and M. Neviere, "Maxwell equations in Fourier space: fast-converging formulation for diffraction by arbitrary shaped, periodic, anisotropic media," *J. Opt. Soc. Am. A* **18**, 2886-2894 (2001).
 19. A. V. Tishchenko, M. Hamdoun, and O. Parriaux, "Two-dimensional coupled mode equation for grating waveguide excitation by a focused beam," *Opt. Quantum Electron.* **35**, 475-491 (2003).
 20. S. BENGHORIEB, R. SAOUDI, and A. V. TISHCHENKO, "Extraction of the 3D plasmon field," *Plasmonics* **6**, 445-455 (2011).
 21. L. D. Landau, L. P. Pitaevskii, and E. M. Lifshitz, *Electrodynamics of Continuous Media (Course of Theoretical Physics S)* (Butterworth Heinemann, 1984).
 22. Y. Saad, *Iterative methods for sparse linear systems* (SIAM, Philadelphia, 2003).
 23. <http://docs.nvidia.com/cuda/cublas>
 24. <https://devtalk.nvidia.com/default/topic/392645/cuda-programming-and-performance/my-speedy-fft-3x-faster-than-cufft/>
-

1. Introduction

Artificial dielectric 3D periodic structures with sub-wavelength periods are promising candidates for replacing natural materials in various optical devices [1-4]. Contrary to band gap crystals, these structures operate in a single mode regime and provide benefits of engineering effective permittivity tensor for specific applications. Currently, 3D periodic photonic crystals with complex period filling are most efficiently produced by the Direct Laser Writing method (DLW, [5]). Despite the reduction of periods towards hundreds of nanometers requires an additional experimental and technological effort, current success in fabrication needs a support in form of reliable effective dielectric tensor simulation and optimization methods. Since the most prominent modification of the effective refractive indices is achieved for high-contrast structures of periods comparable with operation wavelengths, various zero wavevector length limit approximations (e.g., [6-8]) provide insufficient accuracy [9], and a rigorous solution of Maxwell's equations is required at some step of the calculation algorithm.

Rigorous numerical solutions to the homogenization problem for optical 3D periodic structures are obtained conventionally by the same methods as those used for photonic crystal band diagram calculation. Most of these methods rely upon the Fourier decomposition of the Maxwell's equations and subsequent formulation of an eigenvalue problem [10-12] (for more references see [11]). State of the art of Fourier methods [11] for calculation of only few lower bands have complexity of only $O(N \log N)$ and require $O(N)$ storage memory with N being a total number of the Fourier harmonics instead of $O(N^3)$ complexity and $O(N^2)$ storage which are in need for full matrix diagonalization. These parameters can be thought of as almost optimal from the computational requirements viewpoint when searching for effective medium parameters. The method enclosed in this work exhibits the same close to linear numerical behavior, so against this background our research can be considered as seeking for the best rigorous method of photonic crystal homogenization.

In this work we propose an alternative to the mentioned class of Fourier methods. Our formulation relies upon the Generalized Source Method (GSM) developed previously for rigorous grating diffraction simulation [13,14]. This method appeared to perfectly simulate complex shaped 2D dielectric grating diffraction, so we were motivated to extend the GSM to 3D structures. In this first development, we focus only on a general method formulation and its application to the homogenization problem in complex anisotropic dielectric structures.

The paper is organized as follows. First, we define a homogenization problem to solve. Second, we describe application of the GSM to rigorous diffraction calculation in 3D periodic dielectric composites. Albeit the resulting equations are very close to those obtained from conventional treatment of the Maxwell's equations in the differential form [11], we formulate our method as primarily integral one starting from a solution written via dyadic Green's function. This description is followed by representation of our approach to effective dielectric tensor components retrieval. The article ends up with numerical examples and discussion of a perspective work.

2. Artificial dielectric structures

Consider simulation of linear optical response in 3D periodic dielectric structures. An example of such structure is shown in Fig. (1), being a 3D periodic lattice of spheres. Denote structure periods as Λ_α , $\alpha=1,2,3$. Despite the below formulation is rigorous without any assumptions on Λ_α values, we will suppose these periods to be smaller than wavelength λ in numerical examples to support only 0-th propagating diffraction order.

Since we aim at performing our analysis within the optical band, all materials are considered to be nonmagnetic with vacuum permeability μ_0 . Optical permittivity of dielectrics usually varies in range from 1 to ~ 10 . Dielectric permittivity of a composite medium is supposed to be infinitely periodic $\epsilon(\mathbf{r}) = \epsilon\left(\mathbf{r} + \sum_{\alpha=x,y,z} m_\alpha \mathbf{a}_\alpha\right)$ with $|\mathbf{a}_\alpha| = \Lambda_\alpha$ and integers m_α . Rigorous simulation of such 3D periodic structure linear response requires numerical solution of the time-harmonic Maxwell's equations

$$\begin{aligned}\nabla \times \mathbf{E} &= i\omega\mu_0\mathbf{H}, \\ \nabla \times \mathbf{H} &= \mathbf{J} - i\omega\epsilon\mathbf{E}\end{aligned}\quad (1)$$

for given permittivity distribution $\epsilon(\mathbf{r}, \omega)$ supposing temporal variations of all fields and sources to be described by factor $\exp(-i\omega t)$. Eqs. (1) should be solved under boundary conditions consisting in continuity of the tangential electric field and the normal electric displacement components relative to interfaces between different media.

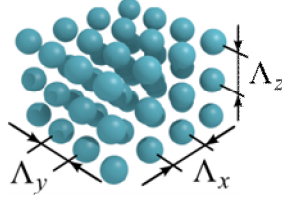


Fig. 1. Example of a 3D periodic dielectric structure. Each period of the structure is supposed to be small enough comparable with light wavelength to support at most two propagating modes in each propagation direction, i.e. to behave as an effective medium.

3. Generalized source method for 3D periodic structures

Before applying the GSM to 3D diffraction simulation and to resolve Eqs. (1), we briefly review the method rationale [15]. The GSM sequentially searches for solutions of Eqs. (1) in the following two steps. First, one chooses a basis problem to replace $\epsilon(\mathbf{r})$ with basis function $\epsilon_b(\mathbf{r})$. The latter should support a known solution to Eqs. (1) for any given source distribution \mathbf{J} : $\mathbf{E} = \mathfrak{N}_b(\mathbf{J})$. At the second step, one goes back to the initial diffraction problem by introducing a generalized source $\mathbf{J}^{gen} = -i\omega[\epsilon(\mathbf{r}) - \epsilon_b(\mathbf{r})]\mathbf{E}$ and substituting it into the basis solution in order to get a self-consistent implicit equation

$$\mathbf{E} = \mathbf{E}_{inc} + \mathfrak{N}_b[-i\omega(\epsilon - \epsilon_b)]\mathbf{E} \quad (2)$$

where \mathbf{E}_{inc} is an initial field excited by real sources in a basis medium with $\epsilon_b(\mathbf{r})$. A proper discretization scheme allows for reducing Eq. (2) to a set of linear algebraic equations which can be solved by efficient iterative methods.

Equation system (1) written in a basis medium with constant permittivity $\varepsilon_b = const$ gives rise to the Helmholtz equation either for the electric field

$$\nabla \times \nabla \times \mathbf{E} - \omega^2 \varepsilon_b \mu_0 \mathbf{E} = i\omega \mu_0 \mathbf{J} \quad (3)$$

or for the magnetic field

$$\nabla \times \nabla \times \mathbf{H} - \omega^2 \varepsilon_b \mu_0 \mathbf{H} = \nabla \times \mathbf{J} \quad (4)$$

With this choice, a basis solution, e.g. for the electric field, becomes the well-known integral solution of Eq. (3) [16]

$$E_\alpha(\mathbf{r}) = E_\alpha^{inc}(\mathbf{r}) + i\omega \mu_0 \sum_{\beta=1,2,3} \int_{V'} \left(\delta_{\alpha\beta} + \frac{1}{k_b^2} \frac{\partial}{\partial x_\alpha} \frac{\partial}{\partial x_\beta} \right) \frac{\exp(ik_b |\mathbf{r} - \mathbf{r}'|)}{4\pi |\mathbf{r} - \mathbf{r}'|} J_\beta(\mathbf{r}') d^3 r' \quad (5)$$

where $k_b^2 = \omega^2 \varepsilon_b \mu_0$, $\delta_{\alpha\beta}$ is the Kronecker symbol, and the multiplier before source $J_\beta(\mathbf{r}')$ is free space dyadic Green's function [16]. With aiming at operating in the reciprocal space decompose Eq. (5) into a plane harmonic spectrum by taking the Fourier transform of both parts:

$$E_{\alpha\mathbf{k}} = E_{\alpha\mathbf{k}}^{inc} + \frac{i\omega \mu_0}{k_b^2} \sum_{\beta=1,2,3} \left(k_b^2 \delta_{\alpha\beta} - k_\alpha k_\beta \right) \left[P \frac{1}{k^2 - k_b^2} + \pi i \delta(k^2 - k_b^2) \right] J_{\beta\mathbf{k}} \quad (6)$$

Here \mathbf{k} is the wavevector of a plane harmonic with components $k_\alpha, \alpha=1,2,3$ and modulo $|\mathbf{k}| = k$; $\delta(k^2 - k_b^2)$ is the 3D Dirac delta-function, and symbol P stands for the integral principal value. Note that the first term in square brackets appears as a particular solution in the reciprocal space of the inhomogeneous scalar wave equation whereas the second term is a general solution of the corresponding homogeneous equation [16,17].

Now we turn to the second GSM step and take the Fourier transform of the generalized current. Product of the permittivity modification by the electric field becomes a convolution product

$$J_{\alpha\mathbf{k}}^{gen} = -i\omega \int \Delta \varepsilon_{\mathbf{k}-\mathbf{k}'} E_{\alpha\mathbf{k}'} d^3 k' \quad (7)$$

where the integration is performed over the whole 3D reciprocal space. Substitution of this current into Eq. (6) gives a particular implementation of Eq. (2) for the considered basis medium and basis solution:

$$E_{\alpha\mathbf{k}} = E_{\alpha\mathbf{k}}^{inc} + \sum_{\beta=1,2,3} \left(k_b^2 \delta_{\alpha\beta} - k_\alpha k_\beta \right) \left[P \frac{1}{k^2 - k_b^2} + \pi i \delta(k^2 - k_b^2) \right] \int \left(\frac{\Delta \varepsilon}{\varepsilon_b} \right)_{\mathbf{k}-\mathbf{k}'} E_{\beta\mathbf{k}'} d^3 k' \quad (8)$$

Sources of external field $E_{\alpha\mathbf{k}}^{inc}$ can be, for example, either a beam refracted at composite structure boundary or dipoles inside the structure. Within the scope of linear theory, the field generated by such sources can be decomposed into plane wave spectrum. Therefore, we can take a plane wave in form $E_{\alpha\mathbf{k}}^{inc} = a_{\alpha\mathbf{k}}^{inc} \exp(i\mathbf{k}^{inc} \cdot \mathbf{r})$ with some wavevector \mathbf{k}^{inc} as the incident field, without loss of generality. Then, recall that due to periodicity the considered class of structures is translational invariant under coordinate shifts along each of three periodicity directions by an integer number of periods. This restricts vector \mathbf{k} to take values only on a discrete 3D periodic mesh with corresponding intervals $K_\alpha = 2\pi/\Lambda_\alpha$. Possible \mathbf{k} component values can be specified by three integers $m_\alpha, \alpha=1,2,3$ constituting vector index

$\mathbf{m} = (m_1, m_2, m_3)$ as $k_{\alpha\mathbf{m}} = k_{\alpha}^{inc} + m_{\alpha}K_{\alpha}$. Under this restriction, Equation (8) becomes an infinite linear algebraic equation system

$$E_{\alpha\mathbf{m}} = \delta_{\mathbf{m}0}E_{\alpha}^{inc} + \sum_{\beta=1,2,3} \frac{k_b^2 \delta_{\alpha\beta} - k_{\alpha\mathbf{m}} k_{\beta\mathbf{m}}}{k_{\mathbf{m}}^2 - k_b^2} \sum_{\mathbf{m}'} \left(\frac{\Delta\epsilon}{\epsilon_b} \right)_{\mathbf{m}-\mathbf{m}'} E_{\beta\mathbf{m}'}. \quad (9)$$

Equation (9) has no delta-term since here and further ϵ_b is supposed to be chosen so that $k_{\mathbf{m}}^2 \neq k_b^2$ for any \mathbf{m} (which is always possible due to denumerability of \mathbf{m} set). Note that the only wavevector governed by the dispersion equation here is $\mathbf{k}_0 = \mathbf{k}^{inc}$, so that $|\mathbf{k}^{inc}|^2 = \omega^2 n_i^2 \mu_0$, where n_i will be a variable in the mode propagation search procedure by means of resonance analysis of solutions to Eq. (9). An analogous equation system for unknown magnetic field is derived from Eq. (4) in a similar manner and writes

$$H_{\alpha\mathbf{m}} = \delta_{\mathbf{m}0}H_{\alpha}^{inc} + \sum_{\beta,\gamma=1,2,3} \xi_{\alpha\beta\gamma} \frac{k_{\beta\mathbf{m}}}{k_b^2 - k_{\mathbf{m}}^2} \sum_{\mathbf{m}'} \left[\delta_{\mathbf{m}\mathbf{m}'} - \left(\frac{\epsilon_b}{\epsilon} \right)_{\mathbf{m}-\mathbf{m}'} \right] \sum_{\sigma,\nu=1,2,3} \xi_{\gamma\sigma\nu} k_{\sigma\mathbf{m}'} H_{\nu\mathbf{m}'}. \quad (10)$$

where $\xi_{\alpha\beta\gamma}$ is Levi-Civita symbol that defines vector product components in Cartesian coordinates.

A finite linear system is obtained from either Eq. (9) or Eq. (10) by truncation. Fourier series truncation is straightforward when coordinate functions $\mathbf{E}(\mathbf{r})$ and $\epsilon(\mathbf{r})$ are smooth. In case of discontinuous permittivity and fields, these equations should be reformulated to avoid products of discontinuous functions with coinciding points of discontinuity before the truncation procedure. This is analogous to what is usually done in the Fourier methods in the diffraction grating theory [13,18]. This reformulation can be performed in 3D periodic structure case also. However, again referring to the diffraction grating theory, use of the mathematically incorrect equation affects the convergence of the method rather than the verity of obtained solutions, and is not critical for pure dielectric structures. Therefore, in this article we rest upon truncated Eqs. (9) and (10) since we are aimed at presenting the method rationale and potential, and will present fine tuning features in a later publication. As it will be seen further even these simplified formulations exhibit quite acceptable convergence for effective parameters retrieval in dielectric structures.

The truncation procedure takes into account only N_x , N_y , and N_z Fourier harmonics along axes X , Y , and Z respectively, and, e.g., transforms Eq. (9) into a matrix-vector equation on unknown electric field component amplitude Fourier images:

$$\sum_{\beta=x,y,z} \sum_{m_x, m_y, m_z} \left[\delta_{\mathbf{m}\mathbf{m}'} \delta_{\alpha\beta} - \frac{k_b^2 \delta_{\alpha\beta} - k_{\alpha\mathbf{m}} k_{\beta\mathbf{m}'}}{k_{\mathbf{m}}^2 - k_b^2} \left(\frac{\Delta\epsilon}{\epsilon_b} \right)_{\mathbf{m}-\mathbf{m}'} \right] E_{\beta\mathbf{m}'} = \delta_{\mathbf{m}0} E_{\alpha}^{inc} \quad (11)$$

Solution of Eq. (11) by an iterative Krylov subspace method like the Stabilized Bi-Conjugate Gradient (BiCGSTAB) or the Generalized Minimal Residual (GMRes) is particularly efficient since the matrix to be inverted here can be multiplied by a vector in a fast manner (we make use of the GSMRes, which is rationalized below). The heaviest procedure here is the multiplication of matrix $(\Delta\epsilon/\epsilon_b)_{\mathbf{m}-\mathbf{m}'}$ by a vector which can be accelerated by the Fast Fourier Transform since Fourier matrix $[\Delta\epsilon/\epsilon_b]$ has Toeplitz structure. Note that we do not make a transform to the coordinate space where multiplication by permittivity is diagonal as it is done conventionally [11]. Instead, we prefer to benefit from analytically found permittivity Fourier components, analogously to [12]. Multiplications define $O(N \log N)$ overall algorithm

computer time and $O(N)$ memory consumption by the whole solution procedure, where $N = N_x N_y N_z$. Details of the fast multiplication can be found, e.g. in our previous publications on the GSM [13,14].

4. Modes in 3D crystals

Eq. (11) (or analogous equation for the magnetic field) being solved provides an amplitude vector for each Fourier harmonic of the field. When an incident wavevector modulo being proportional to n_i at a given frequency approaches a mode propagation constant at a given direction the field response exhibits resonant behavior. This resonance is known to be described algebraically by an isolated complex pole. Then, in order to calculate propagation constants by use of rigorous solutions obtained in accordance with the previous section we represent the 0-th Fourier order response field as a meromorphic function of incident field wavevector modulo $\kappa = |\mathbf{k}^{inc}|$:

$$\xi(\kappa) = \sum_{j=1}^{N_p} \frac{\zeta_j}{\kappa - \eta_j} + \sum_{j=0}^{\infty} \gamma_j \kappa^j \quad (12)$$

The term $\xi(\kappa)$ stands for either electric or magnetic field 0th order vector component amplitude, η_j are propagation constants being poles of $\xi(\kappa)$, ζ_j are modal field amplitudes, and γ_j are constant coefficients in the regular part of the field decomposition. In fact, any diffraction order would possess a similar resonant behavior. The choice of the 0-th order here is most convenient since in the effective medium simulation this order would have the largest amplitudes which would allow for decreasing numerical accuracy loss. In this work, we use an efficient implementation of pole η_j and amplitude ζ_j search algorithm based on the numerical derivation [19,20].

Briefly, the algorithm is as follows. First, a search of propagation constants η_j is reduced to determine polynomial coefficients p_k :

$$P_{N_p}(\kappa) \equiv \prod_{j=1}^{N_p} (\kappa - \eta_j) = \sum_{k=0}^{N_p} p_k \kappa^k \quad (13)$$

Then, product $P_{N_p}(\kappa)\xi(\kappa)$ is an analytic function, and applying to it the N_d -th order Newton divided difference operator in some interval $\kappa_{\min} \leq \kappa \leq \kappa_{\max}$ containing $N_d + 1$ points κ_p ($N_d > N_p$), one gets an approximate equality

$$D_{N_d} [P_{N_p}(\kappa)\xi(\kappa)]_{\kappa_0, \dots, \kappa_{N_d}} \approx 0 \quad (14)$$

Using the explicit expression for the divided difference and choosing $N_p - 1$ independent point sets at interval $\kappa_{\min} \leq \kappa \leq \kappa_{\max}$ one obtains linear equation system for unknown coefficients p_k :

$$\sum_{k=0}^{N_p-1} \left[\sum_{i=0}^{N_d} \frac{\kappa_i^k}{\xi_i \prod_{\substack{j=0 \\ j \neq i}}^{N_d} (\kappa_i - \kappa_j)} \right] p_k = - \sum_{i=0}^{N_d} \frac{\kappa_i^{N_p}}{\xi_i \prod_{\substack{j=0 \\ j \neq i}}^{N_d} (\kappa_i - \kappa_j)} \quad (15)$$

Zeros η_j are found using a standard QR factorization procedure as eigenvalues of the companion matrix of polynomial (13). With propagation constants η_j being found, calculation of pole amplitudes becomes straightforward:

$$\zeta_k = \left[\prod_{\substack{i=1 \\ i \neq k}}^{N_p} (\eta_k - \eta_i) \right]^{-1} \sum_{i=0}^{N_d} \xi_i \prod_{j=1}^m (\kappa_i - \eta_j) \prod_{\substack{j=1 \\ j \neq i}}^{N_d} \frac{(\eta_k - \kappa_j)}{(\kappa_i - \kappa_j)} \quad (16)$$

The described algorithm has two parameters: number of poles N_p , and number of divided difference operator points N_d . Despite each propagation direction in an artificial effective medium can be described by two refractive indices (solutions of the Fresnel normal equation), it is preferable to choose N_p to be greater than 2 for numerical reasons. A good choice of N_p and N_d values for the dielectric tensor calculation was found to be $N_p \sim 5$, $N_d \sim 10$. In this case, pole calculation accuracy is high enough to not affect the convergence of effective dielectric tensor components.

5. Calculation details

An essential part of the method is evaluation of the dielectric permittivity Fourier images. In Fourier-based approaches with a diagonal coordinate space permittivity by field multiplication (e.g., [11]), one uses permittivity evaluated at some spatial mesh points. Implementation of such finite mesh introduces an additional inaccuracy which in turn requires an additional effort to overcome it in form of some boundary averaging procedure [7,11]. We prefer to benefit from analytically known Fourier images of simple shapes as sphere, parallelepiped, or tetrahedron, similarly to [12]. These exact images can be combined to obtain Fourier matrices of most experimentally realizable protonic crystal structures. Explicit expressions for simple solid shapes are well known and can be found elsewhere [12]. Note also that Fourier components of inverse permittivity $[\varepsilon_b/\varepsilon]_{\mathbf{m}}$ within the H-field formulation are found analytically just in the same way as matrix $[\varepsilon/\varepsilon_b]$ components, so there is no need to invert numerically matrix $[\varepsilon/\varepsilon_b]$.

From computational viewpoint, the described method relies mainly on two basic numerical procedures: the GMRes and the Fast Fourier Transform. These two define primarily program time and memory consumption. The reason for using the GMRes instead of, e.g., the BiCGSTAB consists in fact, that the GMRes converges at each point of an equidistant mesh κ_p , $0 \leq p \leq N_d$, even for points being close to poles, whereas other methods fail to converge in the vicinity of poles. Nevertheless, other matrix inversion iterative methods probably could be implemented in the described algorithm, however, this issue lies beyond the scope of this paper and will be discussed elsewhere. Number of GMRes iterations in all examples presented further varied in range from about 10 for low-contrast structures to about 50 for high-contrast structures.

Program based on the described method was implemented for both CPU and GPU calculations. Both programs were written under Windows 7 platform using Microsoft Visual

Studio 2010 Professional edition. GPU program was written in CUDA language for GeForce GTX Titan graphic card. The GMRes algorithm was implemented according to Saad [22] with the modified Gram-Schmidt orthogonalization. Internal vector operations were implemented via CUBLAS procedures [23]. For the FFT we used the Cooley-Tukey algorithm. For GPU computation instead of ready-to-use CUFFT library we used our own FFT implementation which algorithmically is very close to the well-known Volkov FFT code [24] but was optimized for the double precision arithmetic.

Calculations were performed on Intel Xeon E5640 processor, and graphic card GeForce GTX Titan with about 6 Gb of memory. Calculation time comparison example for CPU and GPU simulations is shown in Table 1 (each time is an average over 10 procedure runs). The table demonstrates a tremendous gain provided by the GPU when the Fourier harmonic number exceeds several thousands. It is this gain that becomes a cornerstone of the described rigorous homogenization method and enables extremely efficient effective dielectric tensor rigorous computation. Even when the GPU memory is insufficient to store all GMRes vectors, and an intense memory exchange between GPU memory and RAM is necessary, the GPU program version appears to be more than 30 times faster than its CPU counterpart.

Table 1. Comparison of calculation time for the GSM rigorous 3D diffraction simulation on CPU and on GPU^a

Number of Fourier orders	16×16×16	32×32×32	64×64×64	128×128×128	256×256×256
CPU-version time, s	0.515	4.204	39.047	409.709	3938.634 (~1 hour)
GPU-version time, s	0.166	0.244	0.448	2.184	113.676 (~2 minutes)
Time gain	~3	~17	~87	~188	~35

^aComparison is given for 3D lattice of spheres having refractive index 3 in the air. Each time value is averaged over 10 corresponding procedure runs. For 256×256×256 Fourier orders 6 GB of GPU memory is not enough to store sufficient number of GMRes vectors, and an intense memory exchange between GPU and RAM is required. GMRes converged to 10^{-8} accuracy at about 30 iterations.

6. Numerical convergence

By means of the developed codes, we investigated numerical convergence of the method for different types of lattices. Namely, mode propagation constants and modal field amplitudes were calculated for different number of Fourier harmonics N_o , and an absolute difference of these modal parameters versus the number of the Fourier harmonic was traced. Fig. 2-3 demonstrate the obtained convergence for two types of 3D crystals (cubic and spherical air holes in the host material) with different refractive index contrast for both E- and H-formulations. Refractive index and field amplitude differences demonstrated a very close behavior, so these are their representative values which are laid off along the vertical axis. The figures show that results with an accuracy of order of 10^{-5} can be achieved even for high contrast structures.

Comparing the E- and the H-formulations it is seen that both possess a similar convergence rate, whereas the former provides generally several times better results. From the viewpoint of conventional rigorous methods [11], where the magnetic field formulation provides a substantial improvement in convergence, this may seem uncommon. However, if we look at the form of the generalized source used in our method for the electric field formulation $\mathbf{J}^{gen} = -i\omega(\epsilon - \epsilon_b)\mathbf{E}$ and for the magnetic field formulation $\mathbf{J}^{gen} = -i\omega[1 - (\epsilon_b/\epsilon)]\mathbf{D}$ we can see that they both lead to incorrect Fourier factorization. Thus, both formulations should possess similar convergence rates, which is confirmed by the presented examples.

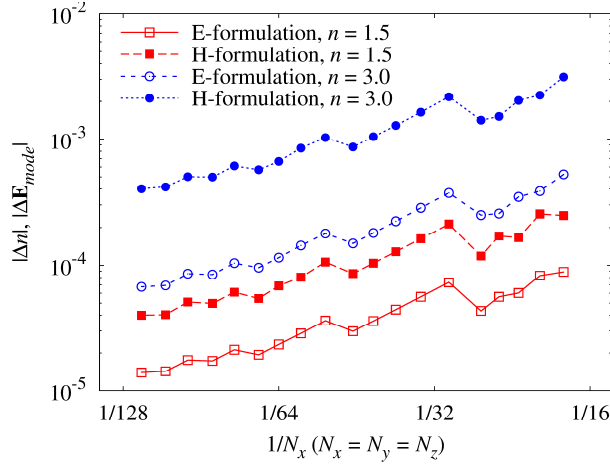


Fig. 2. Convergence of mode propagation constant and modal field for the E-formulation and the H-formulation for a crystal being an infinite 3D periodic set of air cubic cavities in a medium with refractive index 1.5 and 3.0. Periods along all three coordinate axes are the same and equal to 0.3λ , and cube side length is half the period. Resulting effective index is 1.441688 for the host medium with $n = 1.5$ and 2.82503 for the host medium with $n = 3.0$.

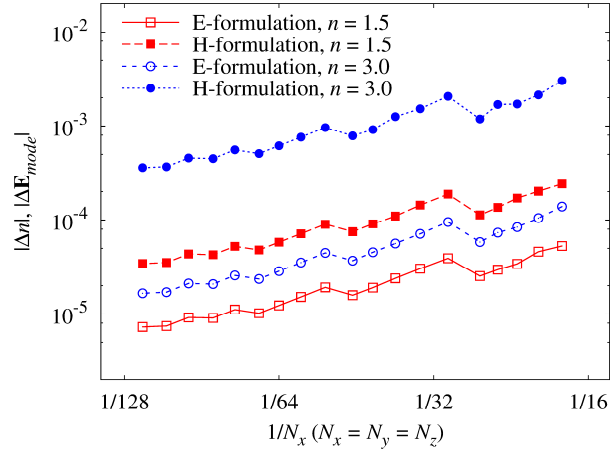


Fig. 3. Convergence of mode propagation constant and modal field for the E-formulation and the H-formulation for a crystal being an infinite 3D periodic set of air spherical cavities in mediums with refractive index 1.5 and 3.0. Periods along all three coordinate axes are the same and equal to 0.3λ , and sphere radius is 0.125λ . Resulting effective index is 1.359786 for the host medium with $n = 1.5$ and 2.53781 for the host medium with $n = 3.0$.

Superiority of the proposed method over quasistatic approaches can be demonstrated by studying effective parameters of 3D periodic composite structures while increasing structure periods. As an example here we consider photonic crystals with effective uniaxial and biaxial behavior. The photonic crystals under consideration are spherical air cavities inside a homogeneous matrix with refractive index 1.5 periodically located along the Cartesian coordinate axes (as in Fig. 1). Uniaxial structure behavior is achieved by letting a period along one axis to be different than the other two, whereas the biaxial behavior is observed when all three periods are different. These lattice types are conventionally referred to as simple tetragonal and simple orthorhombic respectively. Note that due to the structure symmetry the principal refractive index axes coincide in these cases with the Cartesian coordinate axes.

In order to compare simulation results for different periods with a quasistatic solution, which is inherently independent of period, we fix the structure volume filling factor and

alternate structure periods. Under this assumption, the cavity radius would change proportionally to periods. Consider first simple tetragonal lattice crystal with uniaxial effective behavior. Set the sphere radius to be $1/3$ of the period when all three periods are equal, so that the volume filling factor is about $f = 0.155$, and vary the period along X axis Λ_x under conditions $f = const$, and $\Lambda_y = \Lambda_z$. Fig. 4a shows the dependence of ordinary and extraordinary effective refractive indices on the period-to-wavelength ratio Λ_x/λ for increasing cavity radius (0.01λ , 0.02λ , 0.03λ , 0.04λ , and 0.05λ). Black solid line shows the Maxwell-Garnett quasistatic solution equal to $n_{MG,uniaxial} = 1.4213$. The well-known effect of the effective refractive index increase for finite period to wavelength ratios in comparison with the Maxwell-Garnett result can be seen along vertical line $\Lambda_x/\Lambda_{y,z} = 1$, which corresponds to an effective isotropic crystal. For other values of Λ_x/λ the anisotropy causes the propagation constant split, and one of the effective indices for certain directions can become lower than that in the quasistatic limit. Simultaneously, the period increase equally shifts both curves corresponding to ordinary and extraordinary indices in the direction of higher propagation constants. Fig. 4b demonstrates corresponding change of the Fresnel normal surface in form of shifted cross sections of this surface by coordinate planes. Blue solid line shows the cross section for $\Lambda_x/\Lambda_{y,z} = 0.7$ which is in the left hand part of Fig. 4a, whereas cross-section shown by red dashed line is drawn for $\Lambda_x/\Lambda_{y,z} = 1.3$ – the right hand part of Fig. 4a.

Graphs in Fig. 5 are similar to those of Fig. 4 but correspond to orthorhombic lattice type crystal with biaxial effective behavior. Here we fixed ratio $\Lambda_y/\Lambda_z = 1.1$ and alternated Λ_x/Λ_y . Sphere radius was chosen $\Lambda_x/3$ under condition $\Lambda_x = \Lambda_z$ so the filling factor was $f = 0.141 = const$. Dependencies of effective refractive indices $n_{x,y,z}$ along dielectric tensor principal axes from Λ_x/Λ_z ratio are plotted in Fig. 5a for several different cavity radii (0.01λ , 0.02λ , 0.03λ , 0.04λ , and 0.05λ). It is seen that bianisotropy allows one to achieve either superiority of all three principal refractive indices over the Maxwell-Garnett solution ($n_{MG,biaxial} = 1.4284$) or make two of them lower than $n_{MG,biaxial}$. Fresnel surface cross-sections corresponding to the left-hand and the right-hand parts of the graph in Fig. 5a are shown in Fig. 5b demonstrating a shift of the effective crystal optical axis from coordinate plane XY to plane XZ .

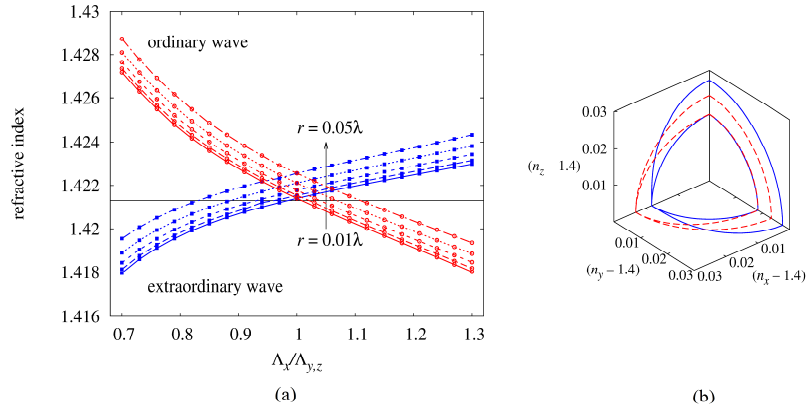


Fig. 4. (a) Ordinary and extraordinary effective indices of a crystal represented by a tetragonal lattice of spherical cavities in a homogeneous matrix with $n = 1.5$ versus the period ratio for increasing cavity radius (0.01λ , 0.02λ , 0.03λ , 0.04λ , and 0.05λ) and constant volume filling factor. Sphere radius is $1/3$ of the period whereas all three

periods are equal. Maxwell-Garnett solution corresponding to the given filling factor is shown by the black solid horizontal line. (b) Cross-sections of shifted normal surface by coordinate planes for the described effective uniaxial crystal corresponding to cavity radius 0.02λ . Blue solid line corresponds to period ratio $\Lambda_x/\Lambda_y = 0.7$, red dashed line corresponds to $\Lambda_x/\Lambda_y = 1.3$.

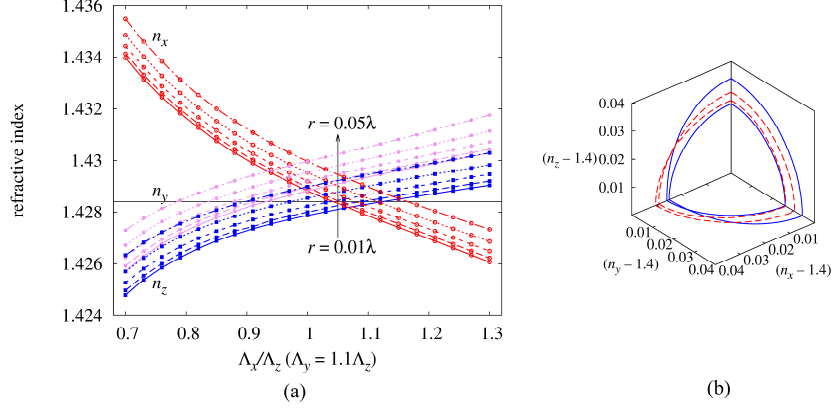


Fig. 5. (a) Effective indices along principal axes of a crystal represented by an orthorhombic lattice of spherical cavities in a homogeneous matrix with $n = 1.5$ versus the period ratio Λ_x/Λ_z under fixed $\Lambda_x/\Lambda_y = 1.1$ for increasing cavity radius (0.01λ , 0.02λ , 0.03λ , 0.04λ , and 0.05λ) and constant volume filling factor. Red curve with circle points corresponds to the diagonal refractive index tensor x-component, magenta curve with filled circles – to y-component, and blue curve with square points – to z-component. Sphere radius is $\Lambda_x/3$ when $\Lambda_x = \Lambda_z$. Maxwell-Garnett solution corresponding to the given filling factor is shown by the black solid horizontal line. (b) Cross-sections of shifted normal surface by coordinate planes for the described effective uniaxial crystal corresponding to cavity radius 0.02λ . Blue solid line corresponds to period ratio $\Lambda_x/\Lambda_y = 0.7$, red dashed line – to $\Lambda_x/\Lambda_y = 1.3$.

7. Conclusion

The article presents the novel sight on the Fourier space methods in 3D photonic crystal analysis and describes the new approach to retrieving effective permittivity tensor of 3D periodic dielectric composites. The new method is referred to as GSM3D and relies upon the GSM developed previously for 1D and 2D diffraction grating simulation. GSM3D includes two principal steps. The first step consists in rigorous electromagnetic solution to the 3D diffraction problem. Obtained rigorous solutions are then used at the second step for resonant analysis of structure response yielding mode propagation constants and modal fields. The mode parameter search was shown to provide accuracy about 10^{-5} and even better for a wide range of refractive index variations. Simultaneously, GPU enabled computations allow for extremely fast analysis of complex crystals which may open a promising way to inverse problem solution concerning effective behavior of complex photonic structures.

Comparing the GSM3D to the previously developed Fourier space methods it should be noted that the present approach possess the same close to linear numerical complexity and computer memory requirements. Additionally, the described resonant analysis is free of issues concerning multiple complex pole search. A future work should include reformulation of the method within the scope of mathematically correct treatment of distribution products and a detailed investigation of its potential.

Acknowledgements

This work was supported by the Ministry of Education and Science of the Russian Federation (no. 16.19.2014/K), Russian Foundation for Basic Research (no. NK 14-07-31352\14), and Russian President Grant for Young Scientists (no. MK-6303.2015.9).